Applied Energy 347 (2023) 121464

Contents lists available at ScienceDirect

Applied Energy

journal homepage: www.elsevier.com/locate/apenergy

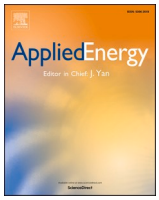

Reducing industrial hydrogen demand through preheating with very high temperature heat pumps

Andrew J. Pimm [a,*], Tim T. Cockerill [a,b], William F. Gale [a]

[a] School of Chemical and Process Engineering, Univ. of Leeds, Leeds LS2 9JT, United Kingdom
[b] School of Mechanical Engineering, Univ. of Leeds, Leeds LS2 9JT, United Kingdom

HIGHLIGHTS

- Reverse Joule-Brayton heat pumps investigated as means of preheating industrial hydrogen.
- Full system optimisation approach developed, including heat exchangers.
- COP estimated to be 1.4–1.7 at 300–500 °C preheat temperatures.
- H_2 demand could be reduced by > 20% by preheating to 500 °C.
- Cost of green H_2 for heating could be reduced by > 10%.

ARTICLE INFO

Keywords:
Water source heat pump
Industrial decarbonisation
Green hydrogen
Geothermal energy
Mine water

ABSTRACT

Decarbonising industry while maintaining economic competitiveness and improving living standards is one of the main challenges of reaching net zero targets, and low-carbon process heating will play a key role in this. In this work we investigate the potential to reduce the energy demands of hydrogen-based industrial heating systems using very high temperature reverse Joule-Brayton cycle heat pumps as preheaters, considering their economics and technical challenges. A thermodynamic process model is used to assess performance at temperatures of 300–500 °C, and cost optimisation is used to conduct cost-benefit analysis of preheating green hydrogen using heat pumps. It is found that over this temperature range, heat pump coefficient of performance lies in the range 1.4–1.7, with the turbine meeting 30–40% of the compressor load. At the electricity prices currently paid by heavy industry in Western Europe, levelised cost of heat from these heat pumps would be less than 4.5p/kWh. Using 500 °C heat pumps as preheaters in hydrogen heating systems could reduce hydrogen demands by over 20% and provide savings on the cost of green hydrogen of at least 8% out to 2050. With process heat accounting for three-quarters of industrial energy use and half of this being at temperatures above 400 °C, these savings are significant and suggest that very high temperature heat pumps could make an important contribution to industrial decarbonisation.

1. Introduction

Industrial decarbonisation is one of the major challenges for governments and organisations seeking to meet net zero emissions targets [1]. Many industrial sectors have a range of promising options to decarbonise production processes, such as fuel-switching and carbon capture and storage, however the route towards decarbonisation of heat supply within industry is currently unclear. Process heat accounts for three-quarters of industrial energy use, with around half of this being at temperatures above 400 °C [2]. In the heavy industries, temperatures can exceed 1,000 °C; such temperatures are typically achieved currently through combustion of fossil fuels, with their associated greenhouse gas emissions. Sectors that involve particularly high process temperatures include basic metals, chemicals, glass, cement, and ceramics, with the majority of the heat demand in those sectors (virtually all in iron and steel) being at temperatures above 500 °C [3,4].

Heat pumps have been widely adopted for relatively low temperature applications, such as space heating in homes and businesses, because of their potential to use low-carbon electricity and lower electricity requirements than resistance heating. However, their adoption within industry for process heat has been limited to date, in part because

* Corresponding author.
E-mail address: a.j.pimm@leeds.ac.uk (A.J. Pimm).

https://doi.org/10.1016/j.apenergy.2023.121464
Received 21 September 2022; Received in revised form 31 March 2023; Accepted 13 June 2023
Available online 22 June 2023

Nomenclature

a	Tube inner radius
A_c	Cross-sectional flow area
b	Tube outer radius
COEP	Coefficient Of Exergetic Performance
COP	Coefficient Of Performance
C	Cost
d	Tube pitch
D	Tube diameter
D_H	Hydraulic diameter
$e_{q,HP}$	Exergy supplied by the heat pump
f_D	Friction factor
h	Heat transfer coefficient
h_i	Enthalpy at state i; Heat transfer coefficient of flow inside tube
h_o	Heat transfer coefficient of flow outside tube
$h_{s,i}$	Enthalpy at compressor/expander outlet after isentropic process
H	Molar enthalpy
k	Thermal conductivity
L	Heat exchanger length
$\dot{m}$	Mass flow rate
n	Lifetime
N	Number of heat exchanger tubes
Nu	Nusselt number
p_i	Absolute pressure at state i
Pr	Prandtl number
q_{HP}	Heat supplied by the heat pump
$\dot{Q}$	Heat transfer rate
r	Discount rate
r_{HP}	Pressure ratio
Re	Reynolds number
s_i	Entropy at state i
T_b	Bulk mean fluid temperature
T_e	Exit temperature
T_i	Absolute temperature at state i; Inlet temperature
T_∞	Ambient temperature
U	Overall heat transfer coefficient
v	Flow velocity
w_C	Work done by the compressor
w_{HP}	Net work done by the heat pump
w_T	Work done by the turbine
γ	Recuperation rate
$\eta_{s,C}$	Isentropic compressor efficiency
$\eta_{s,T}$	Isentropic turbine efficiency
λ	Air-fuel equivalence ratio
μ	Dynamic viscosity
ν	Kinematic viscosity
ρ	Density
ϕ	Fractional fuel saving

their coefficient of performance reduces as sink temperature is increased. To achieve higher temperatures, it is necessary to increase the pressure ratio across the compressor, but this pressure ratio is ultimately limited by the need to avoid icing at the low temperature heat exchanger. This is particularly important for water-source heat pumps, including seawater heat pumps and mine water heat pumps, which benefit from water's high heat capacity and thermal conductivity, the potential for water to be pumped to a heat exchanger, and the relative ease of installing collector loops in water.

Mine water geothermal energy has seen particular interest in recent years due to its potential to provide useful low temperature heat in low-carbon district heating schemes. Mine water heat has already been harnessed in several countries around the world, including Canada, the Netherlands, Spain, and the UK [5]. It has been estimated that one quarter of the UK population lives above abandoned coal mines [6], many of which were left to gradually flood after mining ceased in the 1980 s and 1990 s. This water is heated through natural geothermal processes. As a result of coal's fundamental role in the industrial revolution, heavy industry is often located around former coal mining areas. Of the UK's steel production sites, for example, all but one (the integrated steelworks at Scunthorpe) are located above abandoned coal mines, shown in Fig. 1. Similarly, other currently carbon intensive heavy industries such as cement, glass, and plastics manufacturing are clustered in former coal mining areas such as Teesside, South Wales, and South Yorkshire.

Recent research by the British Geological Survey determined a median geothermal gradient of 24.1 °C/km for the British coalfields [7]. Of interest to UK heavy industry are the mean geothermal gradients in the North East (34.4 °C/km), Yorkshire (32.3 °C/km), Central Scotland (29.8 °C/km), South Wales (19.5 °C/km), and Warwickshire (17.3 °C/km). Practical experience has shown that abstraction of mine water brings deeper warmer water closer to the surface, leading to increased temperatures along the length of the pumping shaft.

Hydrogen has been proposed as a decarbonisation option in several industrial sectors, including steel [8] and glass [9], and hydrogen combustion is being investigated as a means of providing high-

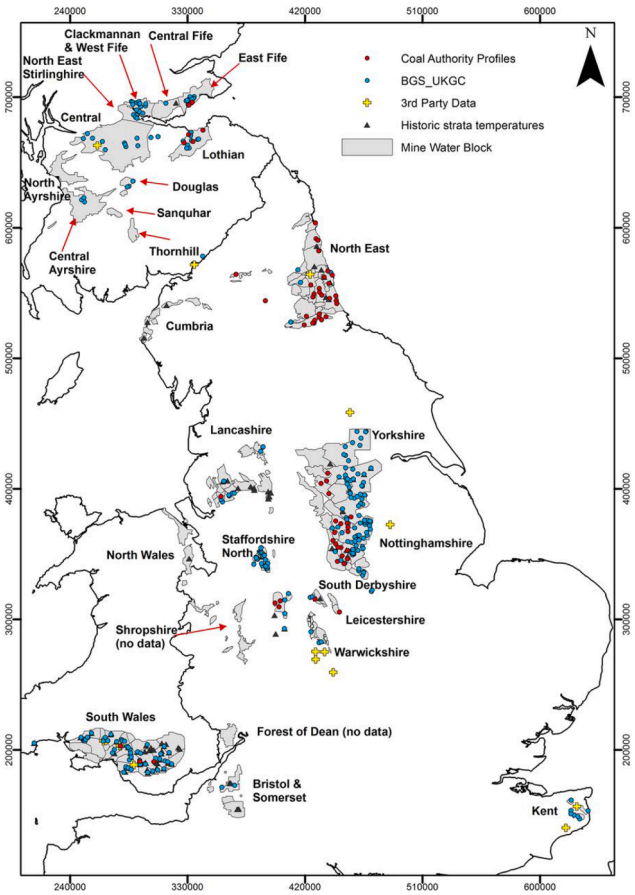

Fig. 1. Location of coalfield mine water blocks in the UK [7].

temperature heat. However, our previous research on hydrogen-based steelmaking has shown that the electricity generation and storage requirements for green hydrogen production in decarbonising industry will be significant [10], with electrolyser efficiencies typically being below 70%. To decarbonise the UK steel industry with green hydrogen, the energy system would need to be expanded by around 4.1 GW of wind capacity, 3.5 GW of solar capacity, and 830 GWh / 0.83 GW of hydrogen storage.

While heat pumps alone are not suitable to reach the extremes of temperature required for many industrial processes (such as the ~ 2,000 °C temperature in blast furnaces), they could be used to preheat combustion air or hydrogen, reducing hydrogen requirements. In turn this would reduce electricity system requirements and production of nitrous oxide, with its considerable global warming potential over a 100 year range being roughly ten times than of methane [11]. Heat pumps could also act as efficient preheaters for other heating systems, such as those based on induction or microwave technology [12,13], and within solid-state hydrogen compression systems based on metal hydrides [14].

Unlike electrical heating systems based on resistive heating, heat pumps absorb heat from the environment and so have coefficients of performance that are greater than one, and typically in the region of 2–5. This can considerably reduce the electricity demands of electrical heating systems. However, heat pumps include moving components (thus increasing maintenance requirements), their coefficient of performance reduces as temperature is increased, and elevated temperature operation requires consideration of thermal expansion (particularly relevant to sealing around moving components).

Heat pumps have typically been considered for low temperature applications in buildings, district heating, and industry, with maximum temperatures of up to around 75–100 °C [15]. However, over the last ~ 10 years, a new field of thermo-mechanical energy storage systems, sometimes known as “Carnot batteries” [16], has developed, whereby heat pumps are combined with thermal energy storage units to form build-anywhere long-duration electricity storage. Of the class of Carnot batteries, pumped thermal electricity storage systems have been proposed involving heat pumps operating at upper temperatures in the range of 500–1,000 °C [17–21], and a test facility has been built at Newcastle University in the UK with an argon heat pump operating at a temperature of 500 °C [22].

Very little attention has been given to the opportunities for such ultra-high temperature heat pumps to reduce the energy demands of low-carbon industrial process heat, even though the scale of energy consumption for industrial heating is vast. Vinnemeier *et al* investigated the thermodynamics of ultra-high temperature heat pumps, studying temperatures from 50 to 700 °C and working fluids of argon, air, and CO_2 [23], however that research did not consider economics or the opportunities for using heat pumps to preheat combustion gases for industrial furnaces (necessary to reach the extremes of temperature required in some industrial processes, such as iron and steel production [3]).

In this paper we investigate the potential for ultra-high temperature water-source heat pumps to reduce energy demand for process heating in industry, covering technical and techno-economic aspects. The proposed system design and analysis methods are presented in Section 2. Analysis results are provided in Section 3, and their wider implications are discussed in Section 4. Finally, we draw conclusions from the research in Section 5.

2. Methods

To investigate the potential of ultra-high temperature heat pumps in industry, we implement a thermodynamic model of a heat pump featuring a recuperator (sometimes known as a regenerator), based on energy balances and constrained nonlinear optimisation, and analyse its performance over a range of temperatures and recuperation rates. We also investigate the economics of these heat pumps when used as a preheater for furnaces running on green hydrogen, using a discounted cash flow approach and accounting for the cost of electrolytic hydrogen production. To perform the economic analysis, we assume that the heat pump costs are dominated by the costs of the turbomachinery and heat exchangers, and so disregard other costs such as balance of plant, providing a lower bound estimate of the heat pump cost. The heat exchanger costs are calculated using heat transfer equations and a nonlinear multivariable optimisation routine that minimises the cost of each heat exchanger.

2.1. Heat pump operating principle and overview of analysis procedure

A heat pump capable of supplying heat at very high temperatures (e.g., 500 °C) while avoiding condensation of the working fluid at the outlet of the expander must make use of a recuperator. A schematic of the proposed concept is presented in Fig. 2, and an example temperature-entropy diagram is presented in Fig. 3. The working fluid circuit is denoted by points 1–6. In this work we assume that the heat pump transfers heat from a water source (such as mine water, as shown in Fig. 2) to an industrial plant, raising the temperature considerably in the process. We recognise that heat pumps can be used in a range of other arrangements, such as upgrading waste heat, and the methods outlined here allow the model to be repurposed for other such analyses.

An electric motor (M) powers a compressor (C) to compress a gaseous working fluid (states 2 → 3), raising its temperature. Heat is supplied from the working fluid to the heat sink (e.g., an industrial plant) through the high temperature heat exchanger (3 → 4). Examples of low-pressure heat transfer media at the industrial plant side could include hydrogen and air (e.g., for preheating prior to combustion). The working fluid then passes some of its remaining heat to the low-pressure side of the circuit via the recuperator (4 → 5) to preheat the low-pressure working fluid prior to compression, before undergoing expansion in turbine T (5 → 6), lowering its temperature considerably. Work is extracted from the turbine, reducing the system’s net work input requirement. The working fluid then extracts heat from the heat source (6 → 1), shown here as mine water, and receives further heat from the high-pressure side of the working fluid circuit via the recuperator (1 → 2), completing the cycle. Other possible heat sources include waste heat, seawater, lakewater, and air.

The recuperator raises the compressor inlet temperature and lowers the expander inlet temperature, reducing the pressure ratio across the

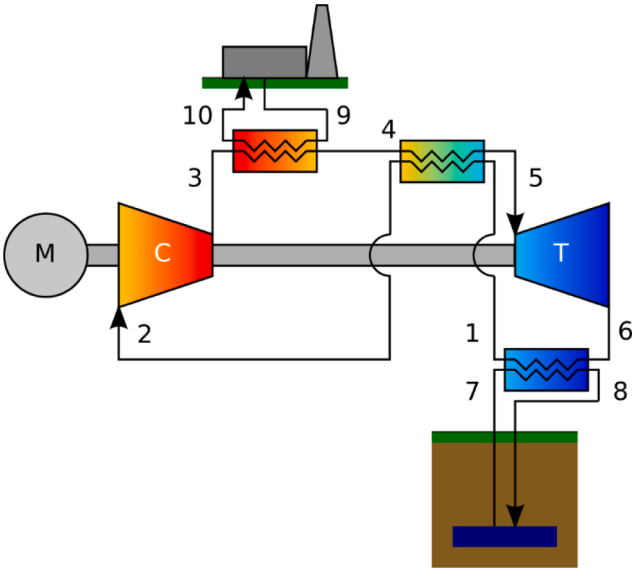

Fig. 2. Schematic of the recuperated mine water heat pump for industrial heating.

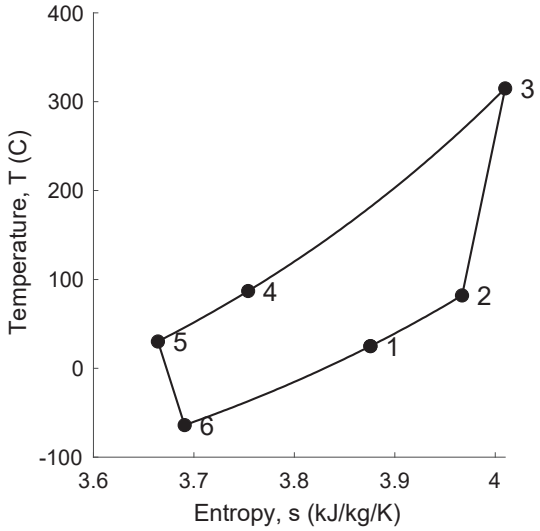

Fig. 3. Temperature-entropy diagram for the recuperated water-source heat pump supplying heat at 300 °C, with argon as the working fluid. Recuperation rate of 0.2. State numbering corresponds with Fig. 2 and is defined in the text.

turbomachinery and ultimately narrowing the heat pump temperature range. This allows very high temperature heat to be supplied while avoiding condensation of the working fluid at the turbine outlet. The recuperated heat pump follows the reverse Joule-Brayton cycle, and is known henceforth as a reverse Joule-Brayton heat pump. A temperature-entropy diagram is shown in Fig. 3 for the heat pump with argon as the working fluid. The temperature increase affected by the recuperator (1 → 2) is clear.

In this paper, we assume single-stage compression and expansion, but recognise that multiple compression and expansion stages could improve performance. The costs and benefits of multi-stage compression and expansion should be investigated in future work.

Evidently, very low temperatures are reached in the working fluid circuit, and in this work we assume that working fluid temperatures are only limited by the higher of the critical temperature and triple point temperature of the gas. Consequently, the working fluid must be dry (to avoid freezing of water vapour in the circuit) and the low temperature heat exchanger must be designed to ensure that the water source does not freeze at the low temperature end. We assume that a drier is used to ensure that the working fluid is kept dry, and our design calculations for the low temperature heat exchanger ensure that the water source temperature remains above freezing.

We recognise that the environmental implications of taking significant quantities of heat from water sources requires further investigation, as does the feasibility of absorbing heat at such low temperatures, particularly with regards to drying of the working fluid (as mentioned above) and dynamic system control schemes that avoid icing in the low temperature heat exchanger. These considerations are deemed beyond the scope of the exploratory work presented here.

The following subsections describe the analysis procedure in detail. In summary, the procedure to design the heat pump and calculate the levelised cost of heat is as follows:

1. **Find temperatures and pressures that maximise heat pump COP. (Sections 2.2–2.3.)** Optimise working fluid temperatures and pressures to maximise heat pump COP while meeting constraints that impose turbomachinery efficiencies and heat balances across the heat exchangers.
2. **Calculate the cost of the heat exchangers. (Section 2.4.)** Considering each of the three heat exchangers separately, optimise the tube inner radius, tube length, and number of tubes based on the working fluid temperatures and pressures found previously. This minimises the cost of each heat exchanger by minimising the mass of steel used, while meeting constraints on total heat transfer and pressure drop on both sides of the tube walls.
3. **Calculate the cost of the turbomachinery. (Section 2.5.)** Calculate turbomachinery cost using the relations in Table 2.
4. **Calculate the levelised cost of heat. (Section 2.6.)** Calculate the total capital expenditure on heat exchangers and turbomachinery, and the annual electricity cost savings, then calculate the net present value of the costs and supplied heat to get to a levelised cost of heat.

2.2. Optimisation problem

To model the heat pump thermodynamics, we take influence from the approach of Vinnemeier *et al* [23] by defining its operation through a set of equations that are framed as constraints in a nonlinear optimisation problem, which seeks to maximise the heat pump's coefficient of performance (COP). This is solved using MATLAB's *fmincon* function. We modify the Vinnemeier model by optimising for COP rather than exergy efficiency and reducing the number of optimisation variables from 32 to 4 (the minimum required). To avoid problems with convergence, we approximate heat exchanger effectiveness using fixed terminal temperature differences.

The optimisation problem can be expressed as

$$\min -COP \tag{1}$$

subject to the constraints

$$r_{HP} = \frac{p_3}{p_2} \tag{2}$$

$$w_C = h_3 - h_2 \tag{3}$$

$$w_T = h_5 - h_6 \tag{4}$$

$$w_{HP} = w_C - w_T \tag{5}$$

$$q_{HP} = h_3 - h_4 \tag{6}$$

$$e_{q,HP} = h_3 - h_4 - T_\infty (s_3 - s_4) \tag{7}$$

$$COEP = \frac{e_{q,HP}}{w_{HP}} \tag{8}$$

$$COP = \frac{q_{HP}}{w_{HP}} \tag{9}$$

$$\eta_{s,C} = \frac{h_{s,3} - h_2}{h_3 - h_2} \tag{10}$$

$$\eta_{s,T} = \frac{h_5 - h_6}{h_5 - h_{s,6}} \tag{11}$$

$$h_4 - h_5 = h_2 - h_1 \tag{12}$$

$$T_1 = T_\infty - \Delta T_{term,LT} \tag{13}$$

$$T_3 = T_{supply} + \Delta T_{term,HT} \tag{14}$$

$$\gamma = \frac{T_4 - T_\infty}{T_3 - T_\infty} \tag{15}$$

$$T_2 = T_4 - \Delta T_{term,re} \tag{16}$$

$$h_i = h(T_i, p_i) \;\; i = 1, \cdots, 6 \tag{17}$$

$$s_i = s(T_i, p_i) \;\; i = 1, \cdots, 6 \tag{18}$$

r_{HP} is the pressure ratio across the turbomachinery, w_C is the work done by the compressor in J per kg of working fluid passing through, w_T

is the work done on the turbine by the working fluid (J/kg), w_{HP} is the net work done by the heat pump (J/kg), q_{HP} and $e_{q,HP}$ are the heat and exergy supplied by the heat pump (J/kg), COEP and COP are the heat pump Coefficient Of Exergetic Performance and Coefficient Of Performance, $\eta_{s,C}$ and $\eta_{s,T}$ are the isentropic efficiencies of the compressor and turbine, T_∞ is the temperature of the heat source, T_{supply} is the temperature at which heat is supplied to the plant on the plant side of the high temperature heat exchanger, ΔT_{term} is the terminal temperature difference at the high temperature ends of the three heat exchangers (low temperature, high temperature, and recuperator), and γ is the recuperation rate.

Specific enthalpies (J/kg) and entropies (J/kg/K) are determined for each state 1–6 based on temperatures and pressures using CoolProp [24], an open-source thermophysical property library.

To reduce the number of optimisation variables to the minimum necessary, we assume that there are only two distinct pressures in the system, p_{hi} (states 3,4,5) and p_{lo} (states 1,2,6), and fix the heat exchanger terminal temperature differences (ΔT_{term}) and the recuperation rate γ so that temperatures at states 1–4 can all be derived from the heat source temperature T_∞ and supply temperature T_{supply}. T_1 and T_3 are derived from T_∞, T_{supply}, $\Delta T_{term,LT}$, and $\Delta T_{term,HT}$ in equations (13) and (14), then T_4 is derived from T_3, γ, and T_∞ in equation (15) and T_2 is derived from T_4 and $\Delta T_{term,re}$ in equation (16).

Consequently, only four optimisation variables are required: p_{hi}, p_{lo}, T_5, and T_6. Wherever these values are set by the solver, all other temperatures can be derived as shown above, therefore all enthalpies and entropies can be derived using CoolProp, and the objective function and constraints functions can all be evaluated. Equality constraints are used to ensure that the isentropic efficiency equations for the compressor and turbine are satisfied (equations (10) and (11)), and that the energy balance across the recuperator is also satisfied (equation (12)). We also use inequality constraints to ensure that w_{HP}, COP, and COEP are always positive and that the optimisation variables are bounded by p_{min}, p_{max}, T_{min}, and T_{max}, as explained in more detail in the following subsection.

The heat pump parameters used in the analysis are given in Table 1.

2.3. Working fluid and additional constraints

In this study we assume that argon is used as the heat pump's working fluid. Argon is inert, sufficiently abundant to make its use practicable, and a monatomic gas at standard temperature and pressure, so has a high heat capacity ratio of 5/3. This means that its temperature increases significantly when compressed. It has been proposed as the working fluid in pumped thermal electricity storage systems for these reasons [17,18,25]. Other candidate working fluids could include air, nitrogen, hydrogen, helium, and neon. Of these, air has the advantage of safety, and turbomachinery for air is widely available, however greater pressure ratios are required than with monatomic gases such as argon, helium, and neon. Energy storage systems have also been proposed based on Rankine cycle heat pumps, with candidate working fluids including carbon dioxide, ammonia, and ethanol [26]. It is expected that supercritical CO_2 will form the working fluid in the next generation of concentrated solar power plants [27], as supercritical CO_2 cycles have high efficiency and compact machinery. Research in supercritical CO_2 heat pumps may prove useful for further development of the ideas presented in this study.

To avoid issues of sealing around a vacuum, all pressures are required to remain above atmospheric pressure. The upper pressure limit is set to 20 MPa to ensure that excessively high pressures do not occur. Liquefaction of the working fluid is avoided by constraining all working fluid temperatures to be at least 20 K above the higher of the critical temperature and triple point temperature, and icing of the water source is avoided by constraining T_8 to be above 2 °C. An upper temperature limit T_{max} of 850 K is imposed, based on the universal "creep cliff" for stainless steels at temperatures of around 873 K [20]. (Depending upon temperatures and the nature of the heat source/sink fluids, it may be possible to use non-stainless steels for some or all of the heat exchangers, however we conservatively assume that austenitic stainless steels are used.) The effect of varying T_{supply} over the range 300–500 °C is examined in the studies that follow. These remaining constraints are given below.

$$101325\text{Pa} \leq p_i \leq 200e5 \text{ Pa } i = 1, \cdots, 6 \tag{19}$$

$$171\text{K} \leq T_i \leq 850 \text{ K } i = 1, \cdots, 6 \tag{20}$$

$$T_8 \geq 275.15\text{K} \tag{21}$$

$$T_{10} = T_{supply} \tag{22}$$

2.4. Heat exchangers

In this study we account for the costs of the three heat exchangers in the system: high-temperature, low-temperature, and recuperator. They are each modelled as counter-flow shell-and-tube heat exchangers, assuming that the heat pump working fluid passes through the tubes in the high-temperature and low-temperature heat exchangers, and that the high-pressure side of the circuit passes through the tubes in the recuperator.

In line with similar analyses in studies of pumped thermal electricity storage systems, we consider only convective heat transfer between the fluids and the inside and outside of the tubes, assuming that any radiation effects are included in the convection heat transfer coefficients, and assuming that the thermal resistance of the tube wall is negligible on the basis that the tube wall thickness is small and the thermal conductivity of the tube material is high.

To ensure that the optimisation procedures remain stable, the heat exchangers are optimised separately after pressures, temperatures, and mass flow rates have been determined with the main heat pump optimisation described above. We recognise that this will not result in the

Table 1
Heat pump parameters.

Turbomachinery		
Isentropic compressor efficiency, $\eta_{s,C}$	80 %	[23]
Isentropic turbine efficiency, $\eta_{s,T}$	90 %	[23]
Working Fluid	**Argon**	
Maximum allowable temperature, T_{max}	850 K	[20]
Minimum allowable temperature, T_{min}	171 K	[23]
Maximum allowable pressure, p_{max}	20 MPa	[23]
Minimum allowable pressure, p_{min}	101.325 kPa	
Heat Source Fluid	**Water**	
Source temperature, T_7	303.15 K	
Minimum allowable temperature, $T_{8,min}$	275.15 K	
Pressure, $p_{7,8}$	101.325 kPa	
Heat Supply Fluid	**Hydrogen**	
Initial temperature, T_9	303.15 K	
Pressure, $p_{9,10}$	101.325 kPa	
Heat Exchangers		
HT-HXU terminal temperature difference, $\Delta T_{term,HT}$	15 K	
Recuperator terminal temperature difference, $\Delta T_{term,re}$	5 K	
LT-HXU terminal temperature difference, $\Delta T_{term,LT}$	5 K	
Maximum allowable pressure drop, Δp_{max}	10 kPa	

Table 2
Turbomachinery cost models [35].

Equipment unit	Sizing factor X	Purchasing cost ($) 2009 basis
Compressor	Shaft power (kW)	$9,000X^{0.6} + 20,000$
Expander (turbine)	Shaft power (kW)	$9,000X^{0.69} + 40,000$

lowest possible cost of heat, however it is necessary to ensure that the optimisation routines converge successfully. We address this separate optimisation of the heat pump and heat exchangers by examining the effects of recuperation rate and pressures on the total cost of heat. We also recognise that the heat pump modelling is relatively simplistic, however we believe that this simplicity is justifiable given the objectives.

We minimise the cost of a given heat exchanger C_{HXU} by solving the following optimisation problem:

$$\min_{a,L,N} C_{HXU} \tag{23}$$

subject to the constraints

$$\Delta p_{tube} \leq \Delta p_{max} \tag{24}$$

$$\Delta p_{shell} \leq \Delta p_{max} \tag{25}$$

$$2\pi aLN \geq \frac{\dot{Q}}{U\Delta T_{LM}} \tag{26}$$

where a is the tube inner radius (shown in Fig. 4), L is the tube length, N is the number of tubes, Δp_{tube} and Δp_{shell} are the pressure drops inside and outside of the tubes, Δp_{max} is the maximum allowable pressure drop, $\dot{Q}$ is the heat transfer rate across the heat exchanger, U is the overall heat transfer coefficient, and ΔT_{LM} is the log mean temperature difference. In this work we set $\Delta p_{max} = 10{,}000$ Pa.

We quantify the cost of the heat exchanger according to the mass of steel that is required. For a shell-and-tube heat exchanger comprising N steel tubes with density ρ_{steel}, each with an inner radius of a, an outer radius of b, and a length of L, the mass of steel is given by

$$m_{steel} = \pi\left(b^2 - a^2\right)LN\rho_{steel} \tag{27}$$

Following the approach of Laughlin [20,28], the heat exchanger cost C_{HXU} is then calculated by doubling the cost of steel

$$C_{HXU} = 2m_{steel}C_{steel} \tag{28}$$

where C_{steel} is the cost of one kg of steel. In this paper we take the density and cost of stainless steel to be $\rho_{steel} = 7{,}900$ kg/m^3 [29,30] and $C_{steel} =$ £2,500/tonne [31], respectively. We fix the tube outer radius to $b = 1.25a$ and the tube pitch to $d = 2.5b$ [20].

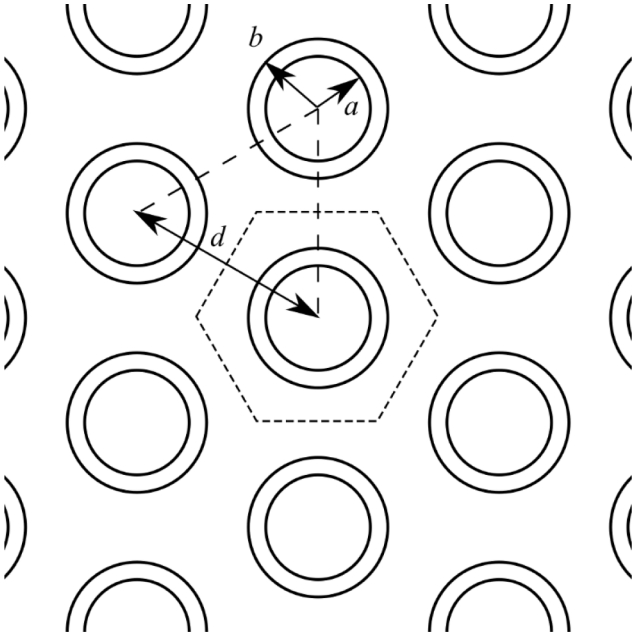

Fig. 4. Cross-section of the tube bundle inside a counter-flow shell-and-tube heat exchanger with triangular pitch, showing tube inner radius a, outer radius b, and pitch d, along with construction lines showing sections used to calculate shell-side cross-sectional flow area corresponding to each tube.

The constraints ensure that pressure drops are below a fixed value Δp_{max} on both the tube side and shell side, and that the heat transfer surface area requirement is met.

Pressure drops on the two sides of the heat exchanger are calculated using the Darcy–Weisbach equation:

$$\Delta p = Lf_D\frac{\rho}{2}\frac{\langle v\rangle^2}{D_H} \tag{29}$$

The fluid densities ρ are determined using CoolProp. When using CoolProp within the heat exchanger calculations, properties are determined at the bulk mean fluid temperature $T_b = (T_i + T_e)/2$, where T_i and T_e are the inlet and exit temperatures of the flow, respectively. The friction factor f_D is determined using the Blasius correlation:

$$f_D = \frac{0.3164}{\mathrm{Re}^{0.25}} \tag{30}$$

where Re is the Reynolds number for the heat exchanger side of interest (given further down). Hydraulic diameters for the two sides are given by

$$D_{H,tube} = \frac{4A_{c,tube}}{2\pi a} = 2a \tag{31}$$

$$D_{H,shell} = \frac{4A_{c,shell}}{2\pi b} \tag{32}$$

where the tube-side and shell-side cross-sectional flow areas associated with each tube in a triangular layout of tubes are given by

$$A_{c,tube} = \pi a^2 \tag{33}$$

$$A_{c,shell} = \frac{d^2\sqrt{3}}{2} - \pi b^2 \tag{34}$$

Mean flow velocity is calculated as

$$\langle v\rangle = \frac{(\dot{m}/N)}{\rho A_c} \tag{35}$$

using the appropriate values of $\dot{m}$, ρ and A_c for the heat exchanger side of interest.

The heat transfer surface area requirement is satisfied using the inequality constraint of equation (26), above. The log mean temperature difference is given by

$$\Delta T_{LM} = \frac{\Delta T_A - \Delta T_B}{\ln\left(\frac{\Delta T_A}{\Delta T_B}\right)} \tag{36}$$

where ΔT_A is the temperature difference between the two streams at one end of the heat exchanger, and ΔT_B is the temperature difference between the two streams at the other end.

Reasonably assuming that the tube wall thickness is small and the thermal conductivity of the tube material is high, the overall heat transfer coefficient can be approximated by

$$U \approx \frac{1}{\frac{1}{h_i} + \frac{1}{h_o}} \tag{37}$$

where h_i and h_o are the convective heat transfer coefficients inside and outside the tubes, respectively.

Convective heat transfer coefficients are derived using the relations

$$h_i = \frac{k_i \mathrm{Nu}_i}{D_{H,tube}} \tag{38}$$

$$h_o = \frac{k_o \mathrm{Nu}_o}{D_{H,shell}} \tag{39}$$

where k_i and k_o are the thermal conductivities of the fluid inside and

outside the tubes (determined using CoolProp) and Nu_i and Nu_o are the Nusselt numbers of the flow inside and outside the tubes.

The Nusselt number both inside and outside the tubes is determined assuming constant surface heat flux when the flow is laminar [32] and using the Gnielinski equation when the flow is turbulent [32,33]. Linear interpolation is used in the transitional flow region, as proposed by Gnielinski [34].

$$\mathrm{Nu} = \begin{cases} 4.36, Re \leq 2300 \\ 4.36 + \dfrac{\mathrm{Re} - 2300}{4000 - 2300}(\mathrm{Nu}_{turb} - 4.36), 2300 < Re < 4000 \\ \mathrm{Nu}_{turb}, Re \geq 4000 \end{cases} \tag{40}$$

The Gnielinski equation for fully developed turbulent flow in smooth tubes is expressed as

$$\mathrm{Nu}_{turb} = \frac{(f_D/8)(\mathrm{Re} - 1000)\mathrm{Pr}}{1 + 12.7(f_D/8)^{0.5}\left(\mathrm{Pr}^{2/3} - 1\right)} \tag{41}$$

Prandtl number Pr is determined using CoolProp.

Reynolds number for the flow inside the tubes is given by

$$\mathrm{Re} = \frac{VD_H}{\nu} = \frac{2\dot{m}_i}{\mu\pi aN} \tag{42}$$

where V is the fluid's velocity, ν and μ are the fluid's kinematic viscosity and dynamic viscosity, respectively, $\dot{m}_i$ is the total mass flow rate of fluid passing through the tubes, and N is the number of tubes.

Reynolds number for the shell flow is given by

$$\mathrm{Re} = \frac{\dot{m}_o D_{H,shell}}{A_{c,shell}\mu N} \tag{43}$$

MATLAB's *fmincon* function is used to find the heat exchanger parameters (a, L, N) that minimise the heat exchanger cost.

While not required in the optimisation problem as laid out here, the diameter of the tube bundle is given by

$$D_{bundle} = 2d\left(\frac{N\sqrt{3}}{2\pi}\right)^{0.5} \tag{44}$$

2.5. Turbomachinery

We evaluate the cost of the turbomachinery using separate compressor and expander unit costs determined using the cost models developed by Morandin *et al* for the analysis of thermo-electric energy storage systems [35,36], provided in Table 2. We apply the cost models at shaft powers of 1 MW and convert from 2009 USD to 2022 GBP using an inflation rate of 1 USD in 2009 = 1.36 USD in 2022 [37] and a mid-2022 exchange rate of 1 USD = 0.84 GBP, resulting in compressor costs of £672/kW and expander costs of £1,254/kW.

These costs are conservative when compared with recent estimations of gas turbine costs published by the UK government's Department for Business, Energy & Industrial Strategy [38], which work out to be £780 per kW of generation capacity. They are also conservative when compared with 2016 cost estimates for the complete charging system of Brayton-based pumped thermal electricity storage systems (reversible heat pump, motor-generator, and other system components such as insulation and controls), which range from €350/kW to €797/kW [39].

2.6. Levelised cost of heat

The levelised cost of heat (LCOH) is the ratio of the total costs of building and operating the heat pump to the total amount of heat that is provided over its life, with both expressed in net present value terms. This is similar to the approach that is widely used to calculate levelised cost of electricity from generation technologies [38], and the approach to calculating levelised cost of electricity which the authors have previously used to evaluate the various options for green steel production [40]. Levelised cost of heat is given by

$$\mathrm{LCOH}_{\mathrm{HP}} = \frac{\mathrm{NPV}_{\mathrm{costs}}}{\mathrm{NPV}_{\mathrm{heat}}} \tag{45}$$

For simplicity, we assume that all components of the heat pump (turbomachinery and heat exchangers) have equal lifetimes of n_{HP} years. At a discount rate r, the net present value of the total costs is given by

$$\mathrm{NPV}_{\mathrm{costs}} = C_{HT} + C_{LT} + C_{regen} + C_{turb} + C_{elec,yr}\left(\frac{1 - (1+r)^{-n_{HP}}}{r}\right) \tag{46}$$

where C_{HT} is the cost of the high temperature heat exchanger, C_{LT} is the cost of the low temperature heat exchanger, C_{regen} is the cost of the recuperator, C_{turb} is the cost of the turbomachinery, and $C_{elec,yr}$ is the yearly cost of electricity to power the heat pump (treated as an annuity in the discounting methodology).

The net present value of the heat provided over the heat pump's life is given by

$$\mathrm{NPV}_{\mathrm{heat}} = 8766\dot{Q}_{HP}\left(\frac{1 - (1+r)^{-n_{HP}}}{r}\right) \tag{47}$$

where $\dot{Q}_{HP}$ is the rate at which heat is provided by the heat pump. We assume that the heat pump operates continuously at full output. In this work we assume a discount rate r of 5% and a lifetime n_{HP} of 30 years.

2.7. Fuel savings

To determine the percentage fuel saving that is achieved by pre-heating a mixture of hydrogen and air, we must assume a given level of excess air. Disregarding carbon dioxide, argon, and the other trace gases, which together comprise less than 1% of air by volume, the combustion reaction is

$$\mathrm{H_2} + 0.5\lambda_{\mathrm{H_2}}(\mathrm{O_2} + 3.76\mathrm{N_2}) \rightarrow \mathrm{H_2O} + 0.5(\lambda_{\mathrm{H_2}} - 1)\mathrm{O_2} + 1.88\lambda_{\mathrm{H_2}}\mathrm{N_2} \tag{48}$$

where $\lambda_{\mathrm{H_2}}$ is the air–fuel equivalence ratio for hydrogen combustion in air. In this work we assume 10% excess air for hydrogen combustion and hence $\lambda_{\mathrm{H_2}} = 1.1$.

Assuming that the hydrogen/air mixture is preheated using the heat pump from T_9 to T_{10}, the preheat per mole of H_2 is given by

$$\begin{aligned} Q_{\mathrm{H_2}} = &\left(H_{\mathrm{H_2}@T_{10}} - H_{\mathrm{H_2}@T_9}\right) + 0.5\lambda_{\mathrm{H_2}}\left(H_{\mathrm{O_2}@T_{10}} - H_{\mathrm{O_2}@T_9}\right) \\ &+ 1.88\lambda_{\mathrm{H_2}}\left(H_{\mathrm{N_2}@T_{10}} - H_{\mathrm{N_2}@T_9}\right) \end{aligned} \tag{49}$$

where H_i is the molar enthalpy of species i at the given temperature, calculated using CoolProp. A lower limit on the fractional fuel saving $\phi_{\mathrm{H_2}}$ is then given by

$$\phi_{\mathrm{H_2}} = \frac{Q_{\mathrm{H_2}}}{\mathrm{LHV}_{\mathrm{H_2}}} \tag{50}$$

where $\mathrm{LHV}_{\mathrm{H_2}}$ is the lower heating value of one mole of H_2 (242 kJ/mol [41]). The lower heating value would not be achieved in reality as the reaction products would not all be returned to 25 °C (e.g., to ensure buoyancy of the nitric oxide-containing waste gases and hence sufficient dispersion from a stack), and so the denominator of this equation would be lower, increasing the percentage fuel saving over that calculated here.

When considering methane combustion, we assume a slightly higher excess air of 15% due to methane's lower flammability limit [42], and hence use $\lambda_{\mathrm{CH_4}} = 1.15$. The combustion reaction, preheat per mole of CH_4, and fractional fuel saving are then given by

$$\mathrm{H_2} + 2\lambda_{\mathrm{CH_4}}(\mathrm{O_2} + 3.76\mathrm{N_2}) \rightarrow \mathrm{H_2O} + 2(\lambda_{\mathrm{CH_4}} - 1)\mathrm{O_2} + 7.52\lambda_{\mathrm{CH_4}}\mathrm{N_2} \tag{51}$$

$$\begin{aligned} Q_{\mathrm{CH_4}} = &\left(H_{\mathrm{CH_4}@T_{10}} - H_{\mathrm{CH_4}@T_9}\right) + 2\lambda_{\mathrm{CH_4}}\left(H_{\mathrm{O_2}@T_{10}} - H_{\mathrm{O_2}@T_9}\right) \\ &+ 7.52\lambda_{\mathrm{CH_4}}\left(H_{\mathrm{N_2}@T_{10}} - H_{\mathrm{N_2}@T_9}\right) \end{aligned} \tag{52}$$

$$\phi_{CH_4} = \frac{Q_{CH_4}}{LHV_{CH_4}} \tag{53}$$

For LHV_{CH_4} we use 802 kJ/mol [41]. We also consider oxy-fuel combustion [43] by removing the N_2 components from the equations, using the same air–fuel equivalence ratios given above.

Parameters relevant to the heat exchanger design, electrolysis, combustion, and economic analysis are given in Table 3.

2.8. Cost of heat from electrolytic hydrogen and heat pumps

To understand the economics of using heat pumps within low carbon industrial heating systems, we assess the hydrogen fuel cost savings achieved by including a reverse Joule-Brayton heat pump in an industrial process heating system based on combustion of electrolytic hydrogen (e.g., green hydrogen). This is accomplished using the fractional fuel saving ϕ_{H_2}, recognising that for every kWh of heat delivered by the system, $(1-\phi_{H_2})$ kWh of heat is provided by the combustion of hydrogen and ϕ_{H_2} kWh of heat is provided by the heat pump. The levelised cost of providing heat via electrolytic hydrogen with heat pump preheating is given by

$$LCOH_{H_2+HP} = (1-\phi_{H_2})LCOH_{H_2} + \phi_{H_2} LCOH_{HP} \tag{54}$$

The levelised cost of hydrogen is determined as

$$LCOH_{H_2} = \frac{NPV_{costs,£/kW}}{NPV_{H_2,kWh/kW}} \tag{55}$$

The net present values are calculated using

$$NPV_{costs,£/kW} = NPV_{electrolyser,£/kW} + 8766 f_{load} \frac{C_{elec,£/kWh}}{\eta_{electrolyser}} \left(\frac{1-(1+r)^{-n_{ap}}}{r} \right) \tag{56}$$

$$NPV_{H_2,kWh/kW} = 8766 f_{load} \left(\frac{1-(1+r)^{-n_{ap}}}{r} \right) \tag{57}$$

Table 3
Parameters used in heat exchanger design and economic analysis.

Heat Pump		
Life, n_{HP}	30 yrs	[20,38]
Compressor cost, C_{comp}	£672/kW	[35,36]
Expander cost, C_{exp}	£1,254/kW	[35,36]
Heat Exchangers		
Stainless steel cost, C_{steel}	£2,500/tonne	[31]
Stainless steel density, ρ_{steel}	7,900 kg/m^3	[29,30]
Minimum allowable tube inner radius, a	1.5 mm	[20]
Tube radius ratio, b/a	1.25	[20]
Tube pitch ratio, d/b	2.5	[20]
Electrolyser		
Life, n_{el}	10 yrs	[41]
Efficiency, $\eta_{electrolyser}$	72 %	[8,41]
Load factor, f_{load}	1	
Combustion		
Air-fuel equivalence ratio for hydrogen combustion, λ_{H_2}	1.10	
Air-fuel equivalence ratio for methane combustion, λ_{CH_4}	1.15	
Lower heating value of hydrogen, LHV_{H_2}	242 kJ/mol	[44]
Lower heating value of methane, LHV_{CH_4}	802 kJ/mol	[44]
Other		
Length of analysis period, n_{ap}	30 yrs	
Discount rate, r	5 %	

where $\eta_{electrolyser}$ and f_{load} are the electrolyser efficiency and load factor, respectively, and n_{ap} is the length of the analysis period in years. As shown in Table 3, we assume an efficiency of 72 % [8,41], load factor of 1, and 30-year analysis period. We also assume an electrolyser lifetime n_{el} of 10 years. $NPV_{electrolyser,£/kW}$ is calculated accounting for investment every time the electrolyser reaches end of life and recuperation of any salvage value at the end of the analysis period, assuming that salvage value reduces linearly to zero over the electrolyser's life. A range of electrolyser capital costs are used in the analysis.

The fractional cost saving from including the heat pump in the system is then given by

$$\theta = 1 - \frac{LCOH_{H_2+HP}}{LCOH_{H_2}} \tag{58}$$

3. Results

3.1. Heat pump performance

The coefficient of performance (COP) and coefficient of exergetic performance (COEP) are shown against recuperation rate and temperature for an argon heat pump in Fig. 5 and Fig. 6. COP generally decreases as temperature and recuperation rate are increased. By contrast, COEP tends to increase with temperature and recuperation rate. Recuperation is a requirement at higher temperatures to ensure that the turbine outlet temperature does not drop below the minimum allowable temperature (set to 20 °C above the critical point of argon) and cause condensation in the turbine.

By way of validation, COP can be compared with that of the Carnot heat pump, given by $COP_{HP,Carnot} = 1/(1-T_L/T_H)$ [45], ensuring that COP is below that of the Carnot heat pump in all cases. It is found that second-law efficiency ranges from 78 % at 300 °C up to 87 % at 500 °C. These values are relatively high compared with those for vapor-compression heat pumps, but the presence of the turbine here (instead of the expansion valve found in vapor-compression heat pumps, which operate over lower temperature ranges and hence lower pressure ranges) reduces both exergy destruction and net power input.

Pressure ratio across the heat pump and the fraction of compressor work that is met by the turbine are shown in Fig. 7 and Fig. 8. Pressure ratio increases with temperature, and recuperation serves to reduce the pressure ratio. At the temperatures considered here, the turbine generally meets 30%-40% of the compressor load, highlighting the importance of using a turbine rather than an expansion valve.

Example heat exchanger details are provided in Table 4, for a 500 °C

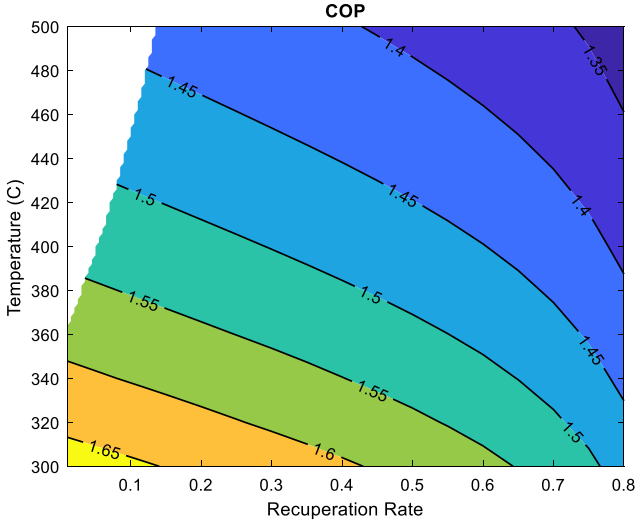

Fig. 5. Coefficient of performance for an argon heat pump.

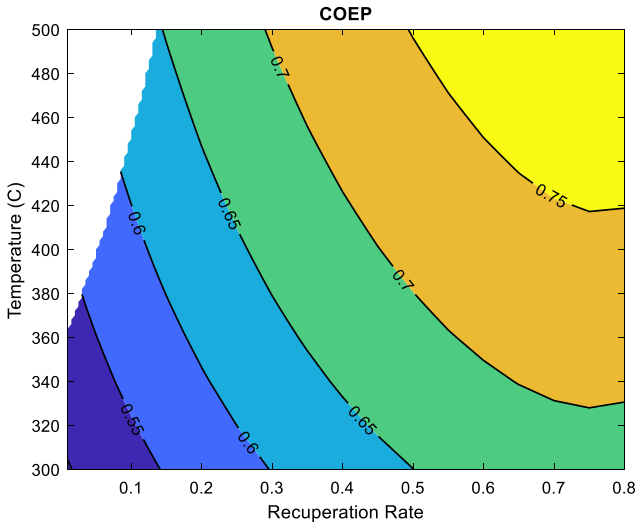

Fig. 6. Coefficient of exergetic performance for an argon heat pump.

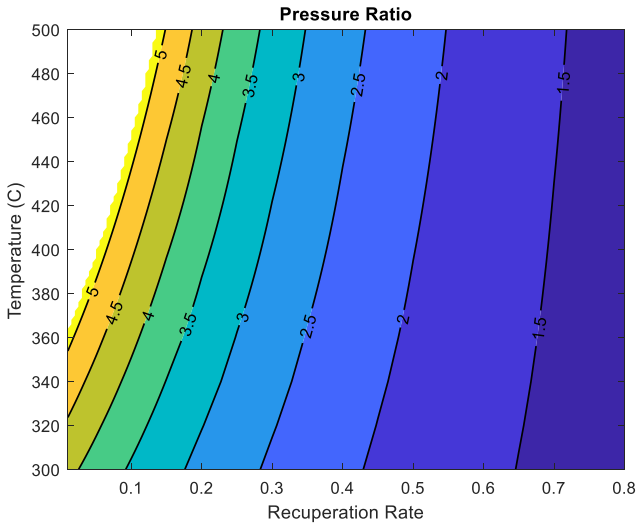

Fig. 7. Pressure ratio across an argon heat pump.

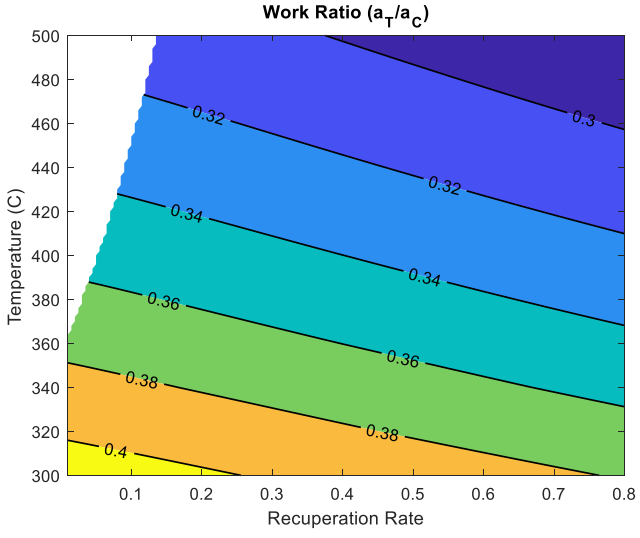

Fig. 8. Fraction of compressor work that is met by the turbine for an argon heat pump.

Table 4
Heat exchanger parameters for a 1 MW 500 °C argon heat pump with recuperation rate of 0.2.

1 MW @ 500 °C	Recuperator	High temperature HXU	Low temperature HXU
Tube inner radius, a	1.5 mm	1.5 mm	1.5 mm
Tube radius ratio, b/a	1.25	1.25	1.25
Tube pitch ratio, d/b	2.5	2.5	2.5
Tube length, L	3.26 m	1 m	1 m
Number of tubes, N	10,000	59,898	50,331
Surface area, A_s	6,153 m^2	1,129 m^2	949 m^2

heat pump with recuperation rate of 0.2. The largest surface area is in the recuperator, even at the relatively low recuperation rate used.

3.2. Levelised cost of heat

At an electricity price of £50/MWh, the levelised cost of heat is shown against recuperation rate and temperature in Fig. 9, and electricity's share of the total levelised system cost is shown in Fig. 10. The levelised cost of heat is minimised by using the lowest possible level of recuperation, and ranges between 3.9p and 4.3p per kWh at the temperatures investigated here. This is lower than the UK government's recent projections of hydrogen cost out to 2050 (5p-7p/kWh for gas reforming with CCS and 4p-20p/kWh for electrolysis) [46]. These results indicate that very high temperature reverse Joule-Brayton cycle heat pumps could provide cost savings to industry by reducing hydrogen requirements, even though their coefficient of performance is relatively low when compared with domestic heat pumps.

At an electricity price of £50/MWh, electricity costs comprise 76–81% of the total levelised system costs when low levels of recuperation are used, making COP the main driver of the cost of heat.

3.3. Potential fuel savings from preheating

It is anticipated that heat pumps could be used to preheat gases for industrial furnaces, and that green hydrogen may be used as the fuel for these furnaces in future. Preheating the burner gases serves to reduce fuel requirements, and the percentage fuel saving is shown against preheat temperature for both hydrogen and methane in Fig. 11,

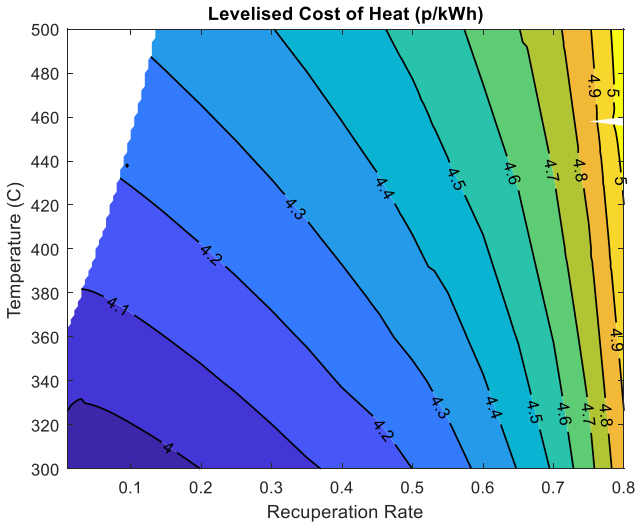

Fig. 9. Cost of heat from an argon heat pump at an electricity price of £50/MWh.

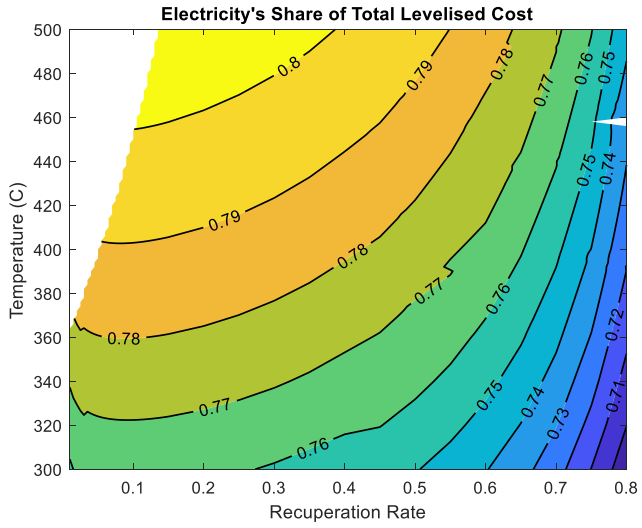

Fig. 10. Electricity's share of total levelised cost for an argon heat pump at an electricity price of £50/MWh.

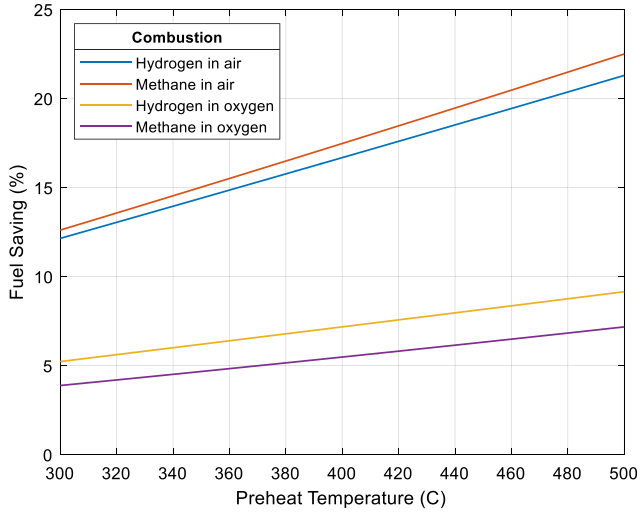

Fig. 11. Fuel saving for hydrogen and methane combustion achieved through preheating from 25 °C.

considering both air and pure oxygen as the oxidant (with the latter approximating oxy-fuel combustion). The fuel savings that could be achieved through preheating to the temperatures considered here are significant, at over 20% for both hydrogen and methane when preheated to 500 °C prior to combustion in air.

Reducing hydrogen requirements consequently reduces the requirements for low carbon power generation capacity, electrolysers, and energy storage. Process heat accounts for three-quarters of industrial energy use, and roughly half of this is at temperatures>400 °C, accounting for around 11% of global energy demand [2]. Therefore the potential for reducing the energy system requirements through the application of high temperature heat pumps in low carbon process heating is significant. Across Europe, the total demand for industrial process heat at temperatures above 500 °C was 999 TWh in 2015 [47]. Therefore very high temperature heat pump preheating could potentially reduce European industrial energy demands by approximately 200 TWh per year. In the UK, the potential demand reduction is approximately 40 TWh/yr.

3.4. Cost savings in combustion of electrolytic hydrogen

At a recuperation rate of 0.2, the cost of hydrogen electrolysis and combustion in air when incorporating a reverse Joule-Brayton heat pump to preheat to 300 °C and 500 °C is shown over a range of electricity prices and electrolyser capital costs in Fig. 12, along with the percentage cost savings achieved through the addition of the heat pump. The cost savings achieved by preheating to 500 °C are also shown against hydrogen cost in Fig. 13, where hydrogen cost is a function of electrolyser capital cost and electricity price varying over the same range as in Fig. 12.

Higher cost savings are achieved by preheating to 500 °C rather than 300 °C. For a given combination of electrolyser capex and electricity price, the relationship between relative cost saving and temperature is found to be linear over the 300 °C to 500 °C temperature range. Adding a reverse Joule-Brayton heat pump to a green hydrogen-based heating system provides cost savings when electricity prices exceed around £5/MWh. At electricity prices above £30/MWh and electrolyser costs above £400/kW, cost savings exceed 5% when preheating to 300 °C and 8% when preheating to 500 °C. In the latter case, savings in the UK would currently be around 10%, and based on recent UK government estimates of the future costs of electricity generation and electrolysers, savings can be expected to exceed 8% out to at least 2050 [38,46]. It has also been found that increasing the discount rate from 5% to 7% and reducing the heat pump life from 30 years to 25 years only reduces the savings to ~7%.

While not shown here, it is found that increasing the heat exchanger terminal temperature differences tends to increase the heat transfer surface area requirement and reduce the COP, thus reducing cost savings. However, these changes are relatively small (particularly the COP reduction) and so they have little effect on the relative cost saving, with capital costs comprising a relatively small proportion of the total cost of heat as demonstrated by Fig. 10.

3.5. Cost comparison with electric boilers

To understand the cost of heating with reverse Joule-Brayton heat pumps relative to electric boilers, the levelised cost of heat from hydrogen combustion in air with electric boiler preheating has been determined and compared with that from heat pump preheating, as shown in Fig. 14. This is based on electric boiler capex and efficiency projections of £113/kW and 98% [48], respectively. Heat pumps become a lower cost option than electric boilers at electricity prices above approximately £25/MWh, with cost savings of over 4% at the very high electricity prices seen in the UK in 2022 (around £180/MWh in Q1 2022 [49]).

4. Discussion

4.1. Coefficient of performance

The results presented above clearly show that using reverse Joule-Brayton heat pumps to preheat hydrogen prior to combustion has the potential to provide meaningful reductions in the cost of low-carbon industrial process heat. This is in spite of what appear to be very low coefficients of performance for heat pumps: 1.7 when preheating to 300 °C, dropping to 1.4 at 500 °C. This suggests a clear avenue for future research into the economics of heat pumps and other competing classes of preheating systems (such as resistance heating).

Heat pumps of the type investigated here feature compressors, expanders, motors, and several heat exchangers; this is clearly a much more complex system than one based on resistance heaters. However, our cost breakdown (Fig. 10) indicates that electricity accounts for a considerable share of the total levelised cost of heat, and so such complexity may be acceptable on the basis that electricity demands for preheating could be reduced by 25%-45% when using heat pumps

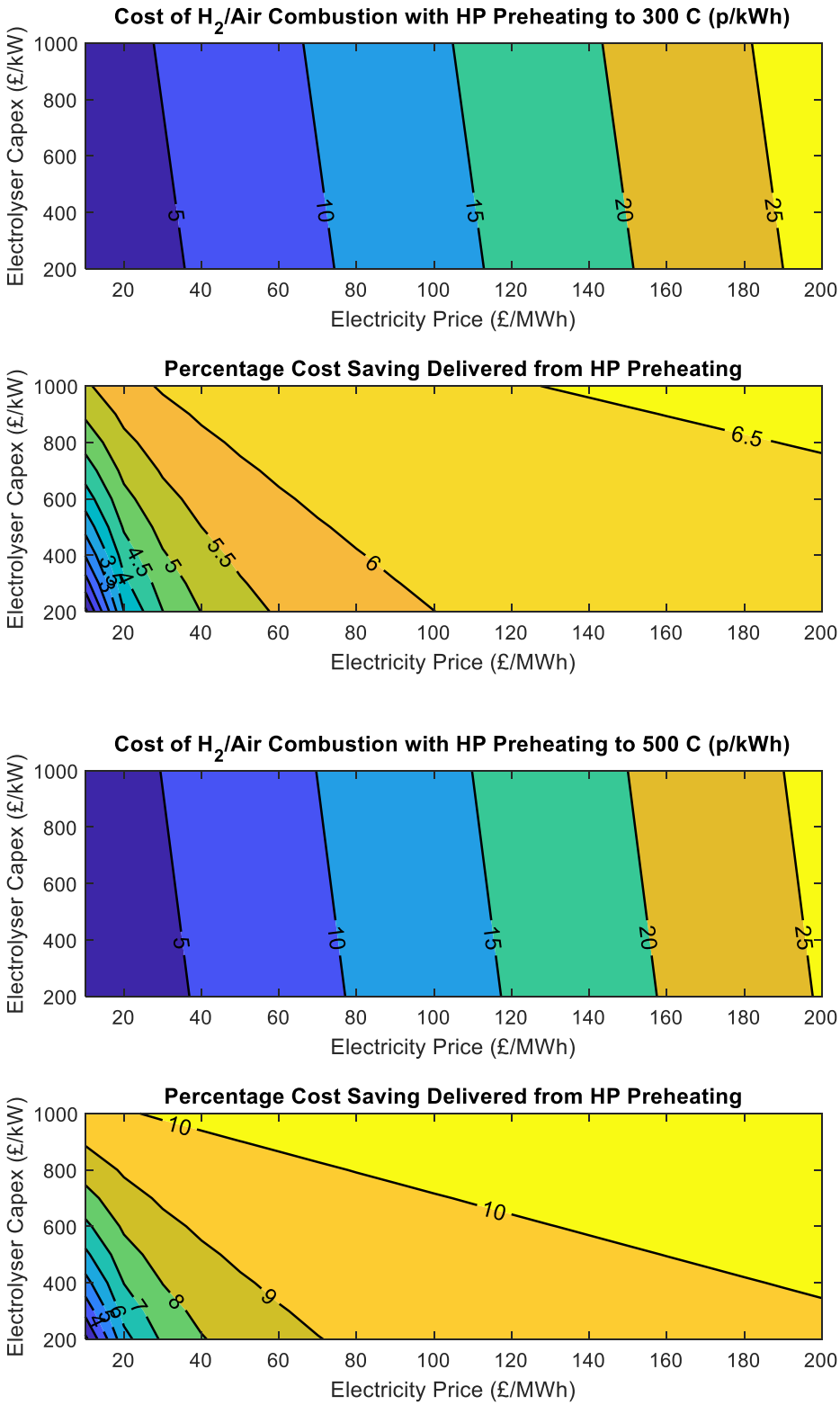

Fig. 12. Effect on the cost of heat from hydrogen combustion from using reverse Joule-Brayton heat pumps to preheat to a) 300 °C and b) 500 °C. Recuperation rate of 0.2.

instead of resistance heaters to preheat to the temperatures considered here.

Moreover, none of the components in Joule-Brayton heat pumps are unproven. Turbomachinery and heat exchangers are widely used in the power generation, aviation, and manufacturing industries, and seawater heat exchangers are used in the maritime and nuclear industries.

4.2. *Working fluid*

In this work we have focused on argon as the working fluid. Argon is a monatomic gas, increasing in temperature significantly when pressurised, and so has been considered by many researchers for pumped thermal electricity storage (PTES) systems [16]. Other gases have also

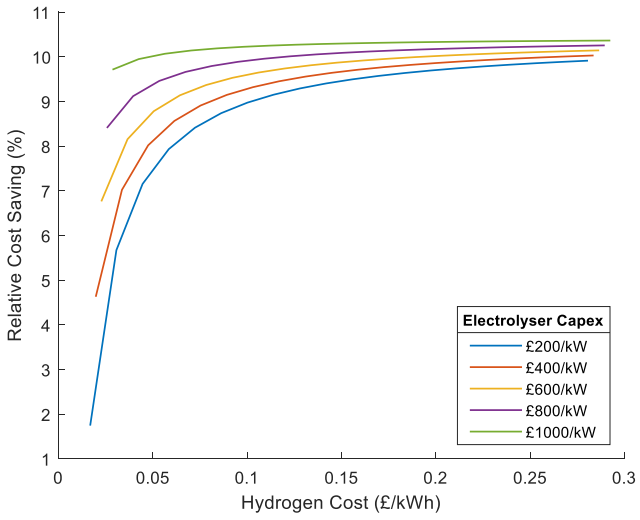

Fig. 13. Percentage saving on cost of hydrogen for air-fired combustion, through hydrogen preheating to 500 °C using reverse Joule-Brayton heat pumps. Recuperation rate of 0.2.

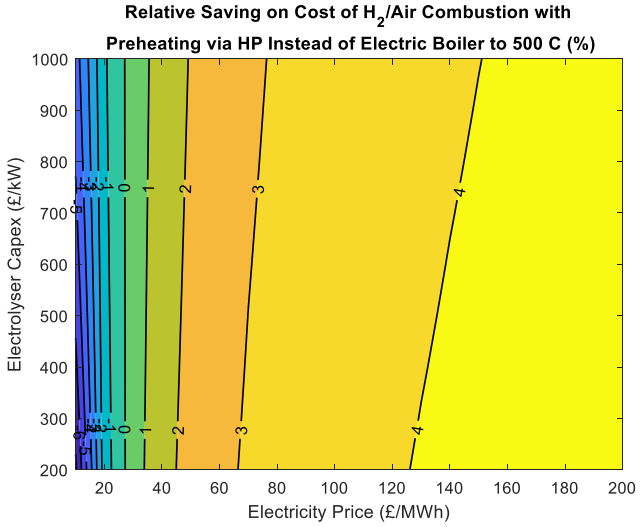

Fig. 14. Percentage cost saving from using heat pump preheating instead of electric boiler preheating (to 500 °C) prior to hydrogen/air combustion, over a range of electrolyser capital costs and electricity prices.

been proposed for PTES systems, including air [50], nitrogen [51], hydrogen [52], helium [53,54], and neon [54]. Recent research by Wang *et al* has shown that helium exhibits lower resistance losses than argon in heat exchangers and thermal storage units [53], and so achieves greater round-trip storage efficiencies. Substituting argon with neon in our heat pump analysis leads to slight increases in coefficient of performance and additional cost savings. However, the differences are small, in the region of 1%. The advantages and disadvantages of candidate working fluids for reverse Joule-Brayton heat pumps should be considered in more detail in future research.

4.3. Potential to integrate thermal energy storage

The motivation for this research stems in-part from recent efforts to advance the field of thermo-mechanical energy storage, particularly pumped thermal electricity storage (within the wider class of thermo-mechanical energy storage systems known as "Carnot batteries" [16]). Within PTES systems, Brayton-based systems (also known as "Brayton batteries" [20]) share many similarities with the heat pump proposed here. Several Brayton-based PTES systems have been proposed with upper temperatures exceeding 500 °C [19,55]. PTES system designs typically feature two thermal energy storage units (one hot store and one cold store), and systems have been proposed based on both sensible heat storage and latent heat storage [56]. In the design developed by Isentropic Ltd. and others in the UK, the hot and cold stores operate at temperatures of around 500 °C and −160 °C respectively [17].

For high temperature storage, solid materials are generally considered over liquids, to avoid issues of phase change and thermal degradation. Vertical packed beds of crushed rock (e.g., basalt, quartz, magnetite, etc.) have been investigated and trialled as storage units by many researchers, with thermoclines being developed by passing the working fluid from top-to-bottom in the hot store and from bottom-to-top in the cold store (though horizontal flow and radial flow packed beds have also been investigated [57,58]). Developments of these systems include layers of different sized storage material [59] and segmentation of the packed bed to minimise exergy losses [60]. To avoid a pressurised hot store, coupled systems have also been proposed whereby the heat/coolth is passed out of the working fluid into separate circuits via heat exchangers [18]. Concrete has been considered for high temperature TES coupled with concentrated solar power, and proven at temperatures up to 400 °C [61–63], and sand is being used as a TES medium in Finland [64]. Multi-tank storage systems have also been proposed for high temperature thermal energy storage, in which a particulate storage material is moved from ambient temperature tanks into high/low temperature tanks [65,66].

The heat pump proposed here is effectively very similar to the Brayton-based PTES system proposed by several researchers [18,25] operating in charge mode and with heat transfer out of the environment and into an industrial plant instead of out of a cold store and into a hot store. As such, a modification of the heat pump could be envisaged whereby a hot or cold store can be charged or discharged as required, such as to take advantage of peak and off-peak electricity pricing. In one configuration, shown in Fig. 15, a hot store might be located on the low pressure side of the high temperature heat exchanger (thus avoiding costs associated with pressure that would be incurred if located on the high pressure side), arranged such that flow through the store can be in

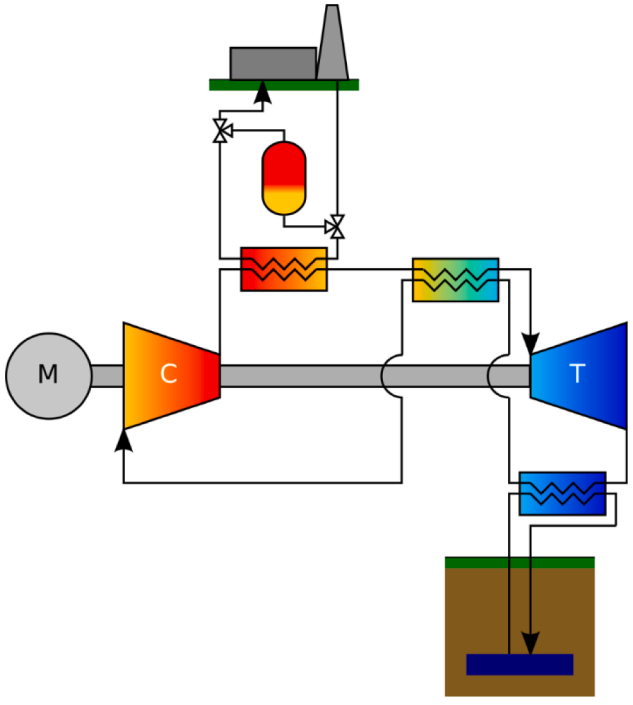

Fig. 15. Modified version of the reverse Joule-Brayton heat pump with the addition of thermal energy storage to improve operational flexibility.

either direction with variable flow rates. This would allow the storage unit to be charged or discharged at variable rates. Alternatively or additionally, a cold store could be incorporated in the system, for example coupled to the outlet of the expander. Further research is needed to investigate the techno-economics of thermal energy storage within industrial process heating systems. Waste materials from industrial processes could potentially be used as thermal energy storage media, such as slag from iron and steel production [67,68]. Unlike battery storage, thermal energy storage systems have low costs per unit of storage capacity (e.g., <€10/kWh [21]), long storage lifetimes, and little to no degradation of the storage or loss of capacity over the system's life.

A cost-benefit analysis of integrated thermal energy storage is deemed beyond the scope of the present work but is worthy of investigation in future. Such analysis could be performed using time series data on electricity prices or renewables availabilities.

5. Conclusions

In this work we have investigated the techno-economics of reverse Joule-Brayton cycle heat pumps as a means of providing very high temperature preheating for industrial process heat, considering preheat temperatures of up to 500 °C. While the coefficient of performance of these heat pumps is relatively low, in the region of 1.4–1.7 over the 300–500 °C temperature range, they can provide meaningful reductions in the levelised cost of heat from hydrogen and natural gas by preheating the combustion gases. Based on current and expected future costs of electrolysers and power generation, it is estimated that cost savings from using these heat pumps to preheat electrolytic hydrogen prior to combustion could be in the region of 10% out to at least 2050.

Heat pumps also appear to be a lower cost preheating option than electric boilers at electricity prices above around £25/MWh, with levelised cost savings on the electric boiler option reaching approximately 4% at electricity prices above £130/MWh, however whether the savings from using heat pumps outweigh their added complexity requires further investigation and should be considered on an application-specific basis.

Heat pump preheating reduces the electricity and natural gas demands of hydrogen-based heating systems, thus reducing capacity requirements for renewables, nuclear, electrolysers, gas reformers, and energy storage. We estimate that preheating hydrogen to 500 °C prior to combustion could reduce hydrogen fuel requirements by over 20%, potentially reducing European high temperature process heating demands by around 200 TWh per year.

Reverse Joule-Brayton heat pumps use existing technologies and components from several areas of industry, including power generation and manufacturing, and they can benefit from the development of pumped thermal electricity storage technologies, with which they share several key features. The commercial deployment of heat pumps as high temperature preheaters rests on further development of turbomachinery and large-scale heat exchangers, along with demonstration at component and system level, however our early indications suggest that the potential to reduce costs and greenhouse gas emissions is considerable.

CRediT authorship contribution statement

Andrew J. Pimm: Conceptualization, Methodology, Software, Validation, Data curation, Writing – original draft, Visualization, Project administration. **Tim T. Cockerill:** Writing – review & editing, Methodology, Supervision, Funding acquisition. **William F. Gale:** Conceptualization, Methodology, Writing – review & editing, Supervision, Project administration, Funding acquisition.

Declaration of Competing Interest

The authors declare that they have no known competing financial interests or personal relationships that could have appeared to influence the work reported in this paper.

Data availability

Data will be made available on request.

Acknowledgments

This research was funded through the EPSRC Centre for Research into Energy Demand Solutions (CREDS, grant reference: EP/R035288/1), to whom the authors are most grateful. We also wish to thank Valerie Dupont of the University of Leeds for providing useful comments on the draft text and input to the calculations on fuel savings, and Bill Nimmo of the University of Sheffield for useful discussions around hydrogen combustion and the effect of preheating.

All data generated in this study are provided in full in the results section of this paper.

References

[1] Garvey A, Taylor P. Industrial Decarbonisation Policies for a UK Net Zero Target. Oxford, UK: Centre for Research into Energy Demand Solutions; 2020.
[2] Philibert C. Renewable energy for industry. Paris: International Energy Agency; 2017. p. 65.
[3] McKenna RC, Norman JB. Spatial modelling of industrial heat loads and recovery potentials in the UK. Energy Policy 2010;38(10):5878–91.
[4] Peakman A, Merk B. The Role of Nuclear Power in Meeting Current and Future Industrial Process Heat Demands. Energies 2019;12:3664.
[5] Limb L. Flooded and forgotten: How Europe's disused coal mines could help heat our homes. 2022. https://www.euronews.com/green/2022/02/14/flooded-and-forgotten-how-europe-s-disused-coal-mines-could-help-heat-our-homes. Accessed on 05 September 2022.
[6] British Geological Survey. New maps reveal heat stored in Britain's abandoned coal mines. 2020. https://www.bgs.ac.uk/news/new-maps-reveal-heat-stored-in-britains-abandoned-coal-mines/. Accessed on 07 October 2021.
[7] Farr G, Busby J, Wyatt L, Crooks J, Schofield DI, Holden A. The temperature of Britain's coalfields. Q J Eng Geol Hydrogeol 2021;54(3).
[8] Vogl V, Åhman M, Nilsson LJ. Assessment of hydrogen direct reduction for fossil-free steelmaking. J Clean Prod 2018;203:736–45.
[9] Doyle A. Trial successfully produces glass using hydrogen power. 2021. https://www.thechemicalengineer.com/news/trial-successfully-produces-glass-using-hydrogen-power/. Accessed on 19 July 2022.
[10] Pimm AJ, Cockerill TT, Gale WF. Energy system requirements of fossil-free steelmaking using hydrogen direct reduction. J Clean Prod 2021;312:127665.
[11] Forster P, Storelvmo T, Armour K, Collins W, Dufresne J-L, Frame D, et al. Chapter 7: The Earth's Energy Budget, Climate Feedbacks, and Climate Sensitivity. In: Masson-Delmotte V, editor. Climate Change 2021: The Physical Science Basis Contribution of Working Group I to the Sixth Assessment Report of the Intergovernmental Panel on Climate Change. Cambridge, United Kingdom and New York, NY, USA: Cambridge University Press; 2021.
[12] Dutta SK, Lele AB, Pancholi NK. Studies on direct reduced iron melting in induction furnace. Trans Indian Inst Met 2004;57:467–73.
[13] Calderon A. Method for direct reduction of iron oxide utilizing induction heating. United States; 1985.
[14] Bellosta von Colbe J, Ares J-R, Barale J, Baricco M, Buckley C, Capurso G, et al. Application of hydrides in hydrogen storage and compression: Achievements, outlook and perspectives. Int J Hydrogen Energy 2019;44(15):7780–808.
[15] Zhang J, Zhang H-H, He Y-L, Tao W-Q. A comprehensive review on advances and applications of industrial heat pumps based on the practices in China. Appl Energy 2016;178:800–25.
[16] Liang T, Vecchi A, Knobloch K, Sciacovelli A, Engelbrecht K, Li Y, et al. Key components for Carnot Battery: Technology review, technical barriers and selection criteria. Renew Sustain Energy Rev 2022;163:112478.
[17] Howes J. Concept and Development of a Pumped Heat Electricity Storage Device. Proc IEEE 2012;100(2):493–503.
[18] Davenne TR, Peters BM. An Analysis of Pumped Thermal Energy Storage With Decoupled Thermal Stores. Frontiers in Energy. Research 2020:8.
[19] Desrues T, Ruer J, Marty P, Fourmigué JF. A thermal energy storage process for large scale electric applications. Appl Therm Eng 2010;30(5):425–32.
[20] Laughlin RB. Pumped thermal grid storage with heat exchange. J Renewable Sustainable Energy 2017;9(4):044103.
[21] Stiesdal. The GridScale technology explained. 2022. https://www.stiesdal.com/storage/the-gridscale-technology-explained/. Accessed on 28 July 2022.
[22] The Engineer. Newcastle University connects first grid-scale pumped heat energy storage system. 2019. https://www.theengineer.co.uk/content/news/newcastle-university-connects-first-grid-scale-pumped-heat-energy-storage-system/. Accessed on 28 February 2023.

[23] Vinnemeier P, Wirsum M, Malpiece D, Bove R. Integration of heat pumps into thermal plants for creation of large-scale electricity storage capacities. Appl Energy 2016;184:506–22.
[24] Bell IH, Wronski J, Quoilin S, Lemort V. Pure and Pseudo-pure Fluid Thermophysical Property Evaluation and the Open-Source Thermophysical Property Library CoolProp. Ind Eng Chem Res 2014;53(6):2498–508.
[25] White A, Parks G, Markides CN. Thermodynamic analysis of pumped thermal electricity storage. Appl Therm Eng 2013;53(2):291–8.
[26] Frate GF, Ferrari L, Desideri U. Rankine Carnot Batteries with the Integration of Thermal Energy Sources: A Review. Energies 2020;13:4766.
[27] McTigue J, Farres-Antunez P, Ellingwood K, Neises T, White A. Pumped thermal electricity storage with supercritical CO2 cycles and solar heat input. AIP Conference Proceedings 2020;2303:190024.
[28] Laughlin RB. Chapter 2 - Mass grid storage with reversible Brayton engines. In: Brun K, Allison T, Dennis R, editors. Thermal. Mechanical, and Hybrid Chemical Energy Storage Systems: Academic Press; 2021. p. 27–64.
[29] Engineering ToolBox. Metals and Alloys - Densities. 2022. https://www.engineeringtoolbox.com/metal-alloys-densities-d_50.html. Accessed on 25 May 2022.
[30] thyssenkrupp Materials. Density of Stainless Steel. https://www.thyssenkrupp-materials.co.uk/density-of-stainless-steel. Accessed on 25 May 2022.
[31] MEPS International. Europe Stainless Steel Price Forecasts. 2022. https://mepsinternational.com/gb/en/products/europe-stainless-steel-price-forecasts. Accessed on 25 May 2022.
[32] Çengel YA, Ghajar AJ. Heat and Mass Transfer: Fundamentals & Applications. 6th ed: McGraw Hill Education; 2020.
[33] Gnielinski V. Neue Gleichungen für den Wärme- und den Stoffübergang in turbulent durchströmten Rohren und Kanälen. Forschung im Ingenieurwesen A 1975;41(1):8–16.
[34] Gnielinski V. On heat transfer in tubes. Int J Heat Mass Transf 2013;63:134–40.
[35] Morandin M, Mercangöz M, Hemrle J, Maréchal F, Favrat D. Thermoeconomic design optimization of a thermo-electric energy storage system based on transcritical CO2 cycles. Energy 2013;58:571–87.
[36] Zhao Y, Song J, Liu M, Zhao Y, Olympios AV, Sapin P, et al. Thermo-economic assessments of pumped-thermal electricity storage systems employing sensible heat storage materials. Renew Energy 2022;186:431–56.
[37] US Inflation Calculator. Inflation Calculator. 2022. https://www.usinflationcalculator.com/. Accessed on 07 July 2022.
[38] Electricity Generation Costs 2020. 2020..
[39] Smallbone A, Jülch V, Wardle R, Roskilly AP. Levelised Cost of Storage for Pumped Heat Energy Storage in comparison with other energy storage technologies. Energ Conver Manage 2017;152:221–8.
[40] Richardson-Barlow C, Pimm AJ, Taylor PG, Gale WF. Policy and Pricing Barriers to Steel Industry Decarbonisation: A UK Case Study. Under consideration with. Energy Policy 2022;168:113100.
[41] Taibi E, Blanco H, Miranda R, Carmo M. Green Hydrogen Cost Reduction: Scaling up Electrolysers to Meet the 1.5°C Climate Goal. Abu Dhabi: International Renewable Energy Agency (IRENA) 2020.
[42] Guarco J, Langstine B, Turner M. Practical Considerations for Firing Hydrogen Versus Natural Gas. https://cea.org.uk/practical-considerations-for-firing-hydrogen-versus-natural-gas/. Accessed on 25 May 2022.
[43] Ilbas M, Bektas A, Karyeyen S. A new burner for oxy-fuel combustion of hydrogen containing low-calorific value syngases: An experimental and numerical study. Fuel 2019;256:115990.
[44] Harrison KW, Remick R, Hoskin A, Martin G. Hydrogen production: fundamentals and case study summaries. National Renewable Energy Lab (NREL), Golden, CO (United States) 2010.
[45] Çengel YA, Boles MA, Kanoğlu M. Thermodynamics: An Engineering Approach. New York: McGraw-Hill; 2020.
[46] Hydrogen Production Costs 2021. 2021.
[47] Fleiter T, Elsland R, Rehfeldt M, Steinbach J, Reiter U, Catenazzi G, et al. Heat Roadmap Europe. Deliverable 3.1: Profile of heating and cooling demand in 2015 -. Data Annex 2017.
[48] Grosse R, Binder C, Wöll S, Geyer R, Robbi S. Long term (2050) projections of techno-economic performance of large-scale heating and cooling in the EU. Luxembourg: Publications Office of the European Union; 2017.
[49] Department for Business, Energy & Industrial Strategy. Prices of fuels purchased by non-domestic consumers in the United Kingdom excluding/including CCL (QEP 3.4.1 and 3.4.2). 2022.
[50] Benato A. Performance and cost evaluation of an innovative Pumped Thermal Electricity Storage power system. Energy 2017;138:419–36.
[51] Wang L, Lin X, Chai L, Peng L, Yu D, Liu J, et al. Unbalanced mass flow rate of packed bed thermal energy storage and its influence on the Joule-Brayton based Pumped Thermal Electricity Storage. Energ Conver Manage 2019;185:593–602.
[52] Garvey SD, Pimm AJ, Buck JA, Woolhead S, Liew KW, Kantharaj B, et al. Analysis of a wind turbine power transmission system with intrinsic energy storage capability. Wind Eng 2015;39(2):149–73.
[53] Wang L, Lin X, Chai L, Peng L, Yu D, Chen H. Cyclic transient behavior of the Joule-Brayton based pumped heat electricity storage: Modeling and analysis. Renew Sustain Energy Rev 2019;111:523–34.
[54] Farres-Antunez P, Xue H, White AJ. Thermodynamic analysis and optimisation of a combined liquid air and pumped thermal energy storage cycle. J Storage Mater 2018;18:90–102.
[55] Benato A, Stoppato A. Heat transfer fluid and material selection for an innovative Pumped Thermal Electricity Storage system. Energy 2018;147:155–68.
[56] Albert M, Ma Z, Bao H, Roskilly AP. Operation and performance of Brayton Pumped Thermal Energy Storage with additional latent storage. Appl Energy 2022;312:118700.
[57] Soprani S, Marongiu F, Christensen L, Alm O, Petersen KD, Ulrich T, et al. Design and testing of a horizontal rock bed for high temperature thermal energy storage. Appl Energy 2019;251:113345.
[58] McTigue JD, White AJ. A comparison of radial-flow and axial-flow packed beds for thermal energy storage. Appl Energy 2018;227:533–41.
[59] Lundgaard C, Engelbrecht K, Sigmund O. A density-based topology optimization methodology for thermal energy storage systems. Struct Multidiscip Optim 2019;60(6):2189–204.
[60] White AJ, McTigue JD, Markides CN. Analysis and optimisation of packed-bed thermal reservoirs for electricity storage applications. Proceedings of the Institution of Mechanical Engineers, Part A: Journal of Power and Energy 2016;230(7):739–54.
[61] Laing D, Lehmann D, Bahl C. Concrete storage for solar thermal power plants and industrial process heat. 3rd International Renewable Energy Storage Conference (IRES III). Berlin, Germany. 2008.
[62] Cabeza LF, Vérez D, Zsembinszki G, Borri E, Prieto C. Key Challenges for High Temperature Thermal Energy Storage in Concrete- First Steps towards a Novel Storage Design. Energies 2022;15:4544.
[63] Ktistis PK, Agathokleous RA, Kalogirou SA. Experimental performance of a parabolic trough collector system for an industrial process heat application. Energy 2021;215:119288.
[64] Energy 2022. Accessed on 15 July 2022, https://polarnightenergy.fi/.
[65] Ma Z, Wang X, Davenport P, Gifford J, Martinek J. Economic Analysis of a Novel Thermal Energy Storage System Using Solid Particles for Grid Electricity Storage: Preprint. 15th International Conference on Energy Sustainability (ES2021). 2021.
[66] SynchroStor. SynchroStor. 2022. https://synchrostor.co.uk/. Accessed on 12 July 2022.
[67] Lopez Ferber N, Al Naimi KM, Hoffmann J-F, Al-Ali K, Calvet N. Development of an electric arc furnace steel slag-based ceramic material for high temperature thermal energy storage applications. J Storage Mater 2022;51:104408.
[68] Haunstetter J, Krüger M, Zunft S. Slag as an inventory material for heat storage in a concentrated solar tower power plant: Experimental studies on design and performance of the thermal energy storage. AIP Conf Proc 2019;2126:200022.